Materials Research. 2023; 26:e20230164
DOI: https://doi.org/10.1590/1980-5373-MR-2023-0164

Electrodeposited Zn-Ni-sisal Nanocrystals Composite Coatings – Morphology, Structure and Corrosion Resistance

A.M.C. Borges[a], G.Y. Koga[b], I.C. Rigoli[c], C.L.F. Rocha[d], P.M.B. Santana[e], C.A.C. Sousa[a]*

[a]*Universidade Federal da Bahia, Programa de Pós-graduação em Engenharia Química, Salvador, BA, Brasil.*
[b]*Universidade Federal de São Carlos, Departamento de Engenharia de Materiais, São Carlos, SP, Brasil.*
[c]*Universidade Federal da Bahia, Instituto de Química, Departamento de Físico-Química, Salvador, BA, Brasil.*
[d]*Universidade Federal da Bahia, Departamento de Ciência e Tecnologia dos Materiais, Salvador, BA, Brasil.*
[e]*Instituto Federal da Bahia-Simões Filho, BA, Brasil.*

Received: March 08, 2023; Revised: June 10, 2023; Accepted: July 03, 2023

Zn-Ni alloys have been used to decrease the corrosion rate of carbon steel substrates. These are used in applications such as bolt coatings, threaded parts, swift valves for gas pipelines, aircraft landing gear, brake system components and others. Zn-Ni coatings containing nanocrystals of cellulose (CNC) obtained from sisal fiber (Sif), a natural polymer, were manufactured using the electroplating technique. Obtaining the nanocrystals involved bleaching raw sisal fiber and then acid hydrolysis to extract the nanocrystal. The effect of the concentrations of the CNC-Sif (0% v/v, 2%v/v, 3%v/v, and 4%v/v) on the morphology and microstructure of the Zn-Ni coating was analyzed through Scanning Electron Microscopy (SEM), X-ray diffraction, and roughness measurements using confocal microscopy. The effect of the addition of CNC-Sif on the efficiency of galvanostatic deposition was analyzed. The corrosion rate through mass loss and electrochemical tests were also analyzed. The effect of adding CNC-SIF on coating microhardness investigated. This study show that the addition of nanocrystals alters the structure, the morphology, increases current efficiency and the corrosion resistance of the Zn-Ni coating and these effects are more significant with the addition of 2% v/v. The results obtained indicate that the addition of the CNC-Sif in the Zn-Ni coating is promising, because it reduces the energy consumed during the electrodeposition process in addition to increasing corrosion resistance of the Zn-Ni and the microhardness.

Keywords: *Sisal Nanocrystals, Electroplating, corrosion, morphology, structure.*

1. Introduction

Zinc coatings obtained through electroplating are widely used to protect the substrate against corrosion due to the barrier effect and cathodic protection. However, in highly corrosive environments like marine or polluted atmospheres, the corrosion rate of zinc is considerable, imposing significant constraints on the applicability of zinc coatings. Furthermore, in these media, the corrosion rate of zinc is much higher than that of the steel substrate[1]. Therefore, it is possible to increase the useful life of the zinc coating and maintain its ability to cathodically protect the steel substrate. Apart from the inclusion of organic additives, there exist several possibilities to enhance the corrosion resistance of zinc coatings include imparting superhydrophobic properties to the metal surface, incorporating nanoparticles, and introducing Ni or Fe into the coating. The corrosion resistance of zinc coating is also affected by the electroplating method. It has been found[2] that pulse reverse curent (PRC) results in a zinc deposit with corrosion resistance superior to that of the coating obtained through direct current and pulsed current. This effect is attributed to obtaining a compact corrosion product beyond the structure of the PRC deposit.

It has been found[3] that the superhydrophobic properties of zinc coating can be obtained by subjecting the coating to an ultrasonic treatment with stearic acid. This procedure is done after electrodeposition from sulfate-acetate solution. The introduction of superhydrophobic properties resulted in an increase in the corrosion resistance of the zinc coating in 0.5 M NaCl which is attributed to a gas interlayer on coating surface in aqueous solutions.

Electrodeposited nanocomposites consisting of a metallic coating with ceramic nanoparticles for use as a protective coating on steel substrates have been widely studied in recent years. It has been found that the corrosion resistance of zinc coating improves with the addition of various nanoparticles such as graphene oxide (GO)[4], SiC[5], TiO2[6], Al2O3[7], and cellulose nanocrystals (CNC) obtained from soybean hulls[8] and cotton fibers[9]. This effect is mainly related to the increased compactness of the deposit and the occurrence of a physical barrier caused by the presence of nanoparticles.

Regarding the addition of Fe, it has been found[10] that the corrosion resistance of zinc coating in NaCl solution increases with the presence of 14wt% of Fe. This effect is related to the presence of the Γ1-Fe5Zn21 phase.

*e-mail: alexandre.magno1411@gmail.com

However, Zn-Ni coatings are the main Zn-based alloys from electroplating. These coatings are used in applications such as bolt coatings, threaded parts[11], swift valves for gas pipelines, aircraft landing gear, and auto parts including fuel transport lines and brake system components. The addition of nanoparticles to Zn-Ni alloys enhances their corrosion resistance and improves the cost/benefit ratio of the material as it reduces the amount of costly Ni needed to provide adequate corrosion resistance. It has been found that the corrosion resistance of a Zn-Ni coating increases with the addition of ceramic nanoparticles such as WC[12], Fe_2O_3[13], TiO_2[14], Al_2O_3[15], SiO_2[16], and CeO_2[17].

In the galvanostatic electrodeposition process, the current efficiency is important from a practical point of view, since a higher deposition efficiency implies a lower energy consumption. However, there is little information in the literature about the effect of adding ceramic nanoparticles on the current efficiency of Zn-Ni coating. Roventi et al.[18] found that the addition of ZrO_2 and $Al2O_3$ in the alkaline bath at concentrations of 5 g/L and 10 g/L does not result in a significant change in the current efficiency of a Zn-Ni coating, and the results are within the margin of error. However, in the deposition of Zn from an alkaline bath it was found[19] that the addition of SiC nanoparticles decreases the current efficiency. This effect is attributed to the change in the reduction potential of hydrogen ions, resulting in an increase in the H_2 partial current, which causes a decrease in the current efficiency. These results therefore show that the effect of ceramic nanoparticles on current efficiency depends on the nature of the nanoparticles.

The superior corrosion resistance of a Zn-Ni coating resulting from the incorporation of ceramic nanoparticles in the coating is attributed to the filling of defects by the nanoparticles, making the alloy matrix more uniform[13,14], and to the decrease in the active surface in contact with the corrosive medium[15]. Apart from the addition of ceramic nanoparticles, other materials of nanometric dimensions may fill defects in the alloy matrix, and being electrically neutral and stable in the corrosive solution, they may also promote an increase in the corrosion resistance of the coating. Among such materials cellulose nanocrystals (CNC) stand out. These materials are obtained from various natural sources and the fibers undergo a process that involves the removal of the amorphous structure, usually through acid hydrolysis[20-22].

Cellulose nanocrystals have the advantage of coming from renewable and low-cost products, and as well as being environmentally friendly, they are easy to process and have low density. In addition, they exhibit a favorable mechanical behavior, high hydrophilicity and lipophilicity, and great emulsification stability. These characteristics make the use of CNC promising for a wide range of applications that include biomedical and pharmaceutical applications, such as their use in delivery vehicles for anticancer agents and their use as a reinforcement phase of polymer matrices[23,24]. However, there is little information about the effect of these nanocrystals on metallic coatings obtained by electrodeposition. To the best of our knowledge, studies on this effect are limited to those on the addition of CNC obtained from cotton fiber[9] and soybean hulls[8]. These studies show that the addition of such CNC decreases the corrosion rate of the coating and this effect is mainly related to the decrease in the roughness of the coating due to the penetration of nanocrystals into the surface defects of the coating. The decrease in the corrosion rate is also related to the CNC acting as an inert barrier resulting in a decrease in the active surface area of the coating.

Various cellulosic materials can be used to obtain CNC, such as sisal fiber, cotton fiber, soy husks, wood pulp, jute, hemp and flax[25-29]. Due to its high cellulose content (50% to 74%), sisal fiber, which is obtained by defibrillation through the sisal leaf, is a promising source of CNC[30]. Furthermore, sisal is the main hard fiber produced in the world, and it is an agricultural product of great socioeconomic importance in several producing countries such as Brazil[31]. It is also important therefore to carry out studies on new applications of sisal fiber in order to add value to this product.

Studies on CNC obtained from sisal fiber (CNC-SiF) mainly involve the effect of the incorporation of these nanocrystals as a reinforcement phase of a polymer matrix. These studies show that the incorporation of CNC-SiF into a polymer matrix can improve the mechanical strength and toughness of the composite, however, this effect depends on the type of polymer matrix used. It was found[32] that the incorporation of CNC-SiF, at levels of 5 and 10 wt%, results in a 100% increase in the modulus of the matrix consisting of waterborne polyurethane (WBPU), and that the elongations are maintained at around 65%. On the other hand, it was found[28] that the incorporation of CNC-SiF at 3 wt% in the polypropylene matrix increases the tensile strength and the modulus around 4.40% and 7.16%, respectively, while the impact strength increases by 21.96 J/m^2 to 24.2 J/m^2. However, there are no published references on the effect of the addition of CNC-SiF on the characteristics of metallic coatings.

In addition to being inert nanocrystals obtained from a renewable natural product and relatively low cost, it is interesting to investigate the effect of adding CNS-SiF to a metallic electrodeposit. Thus, in the present work, a comparative analysis was made to investigate the effect of adding cellulose nanocrystals obtained from sisal fiber on the morphology, microstructure, and deposition efficiency of a Zn-Ni coating. The effect of the addition of these nanocrystals on the coating corrosion resistance is also investigated.

2. Experiments and Methods

2.1. Production and characteristics of the nanocrystal of sisal fiber

Obtaining the nanocrystals of sisal fiber (CNC-Sif) involved bleaching raw sisal fiber and then subjecting it to acid hydrolysis to extract the nanocrystal[33].

In the first stage of bleaching, around 10.0 g of the ground and sieved fiber (16 mesh) was put into a beaker containing 200 mL of sodium hydroxide solution (5% NaOH, w/v) at a temperature of 90 °C. The system remained under constant agitation for 90 min. After cooling, filtration was carried out under a vacuum. The retained solid material was washed with distilled water until a neutral pH was reached. The fiber was dried in an oven with air circulation at 50 °C until it reached a constant weight.

In the second stage of bleaching, the fiber was put into a mixture of sodium hydroxide solution (NaOH, 5% w/v), glacial acetic acid PA (CH_3COOH, 5% v/v), and sodium hypochlorite (NaClO, 2 and 5% (v/v), at a temperature of 80 °C). The system remained under constant agitation (600 rpm) for 120 min. After cooling, filtration was carried out under vacuum, washing the material with distilled water until reaching a pH 7. The fiber was dried in an oven with air circulation at 50 °C until a constant weight was reached. This bleaching step was repeated three times.

To extract sisal cellulose nanocrystals, the bleached fibers (5.0 g) were subjected to acid hydrolysis in a sulfuric acid solution (100 mL H_2SO_4 56% v/v) under vigorous stirring at 60°C for 30 min. The resulting suspensions underwent 11 centrifuges of 10 min and 3400 rpm. After this step, the solution was resuspended in 500 mL of distilled water and dialyzed in water to remove excess acid (pH between 6 and 7). After neutralization, the solution was ready for use in the electrolytic bath. The characteristics of the nanocrystals are listed in Table 1. Zeta potential was determined at 25 °C using a Malvern Nano-ZS apparatus. Three measurements were performed. The dimensions of the nanocrystals were obtained using transmission electron microscopy (TEM, Tecnai™ G2 F20) with the help of Image J software and 50 measurements were computed[33]. Measurements show that the sisal nanocrystals exhibit a whiskers shape with nanometric dimensions.

The results reported in Table 1 show that nanocrystals have a potential Zeta value of less than -30 mV, generally considered the limit between uncharged and charged particles[34].

2.2. Bath deposition and electrodeposition process

Zn-Ni coating was obtained from an acid bath (pH = 3.5, the composition of which is detailed in Table 2[35]. Initially, coatings were obtained in the absence and presence of the following concentrations of CNC-Sif added to the deposition bath: 1% v/v, 2% v/v; 3%v/v; and 4% v/v. For a CNC-Sif concentration of 5% v/v, the adhesion of the coating to the substrate was not adequate. On the other hand, the addition of 1% v/v of the CNC-Sif was not enough to change the corrosion rate of the Zn-Ni coating obtained through mass loss therefore the effect of the addition of this concentration was not analyzed in the other tests.

The coating was deposited at room temperature without agitation, using AISI 1020 carbon steel as substrate. The depositions were carried out at a current density of 10 mA/cm^2 applied for 18.5 min, resulting in a coating with a thickness of 5 µm. As a counter electrode (anode) a 5 mm diameter graphite bar was used.

Table 3 lists the pH and electrical conductivity values at 25° C for the deposition bath in the absence and presence of different concentrations of the CNC-Sif.

2.3. Analysis of morphology and structure

A scanning electron microscope (SEM, model Quanta 400 FEI) equipped with an energy dispersive spectrometer (EDS) detector was used to analyze the morphology and composition of the Zn-Ni coatings. The topographic images and the surface roughness of the coating were obtained by laser scanning confocal microscopy (LSCM) using the Olympus model LEXT OLS4100 equipment. The roughness parameters considered were: Sa (arithmetic mean of the absolute value of the surface departure above and below the mean plane within the sampling area, this parameter is used generally to evaluate surface roughness), Sp (height of the highest peak within the defined area), and Sv (depth of deepest valley within the defined area).

The parameter S_a was determined through the following Equation 1[36]:

Table 1. Characteristics of CNC-Sif, where L corresponds to the length, and D to the diameter of the nanocrystals[25].

Crystallinity Index (%)	Zeta Potential (mV)	L (nm)	D (nm)	(L/D)
78	-25.2 ± 0.7	210 ± 60	5 ± 2	42

Table 2. Composition of bath deposition used to obtain the Zn-Ni coating.

Component	Concentration (mol/L)	Function
$ZnCl_2$	0.28	Source of Zn
$NiCl_2.2H_2O$	0.15	Source of Ni
NH_4Cl	2.80	Increases the conductivity of bath deposition
H_3BO_3	0.32	Buffer solution

Table 3. pH and electrical conductivity of the deposition bath without and with different nanocrystal concentrations.

Nanocrystal Concentrations (% v/v)	pH	Electric Conductivity (mS/cm^2)
0	4.52	139.1
2	4.52	139.5
3	4.51	140.1
4	4.45	142.5

$$S_a = \frac{1}{A}\iint_A |z(x,y)|\,dxdy \quad (1)$$

where: A represents the defined scanning (or observation) area, and x, y, z correspond to the coordinates of length, width, and height, respectively.

The coating structure was determined by X-ray diffraction (XRD) analysis, using a Bruker D8 Advance ECO, with Cu-Kα-1 radiation (1.54 Å / 8.047 keV). From the XRD diffractograms, the relative texture coefficient (T_C), the size of the crystallites, and the microstrain of the Zn-Ni coating were determined.

The texture coefficient (Tc) was obtained using the following Equation 2[37]:

$$T_C(hkl) = \frac{I_{(hkl)} / I_{0(hkl)}}{\frac{1}{n}\sum I_{(hkl)} / \sum I_{0(hkl)}} \quad (2)$$

where: $I_{(hkl)}$ is the peak intensity of Zn-Ni coating, $I_{0(hkl)}$ is the intensity of peaks of standard Zn-Ni powder sample, taken from JCPDS file card number 47-1019, and n is the number of peaks present in the diffractogram.

The Debye–Scherrer Equation 3 was used to calculate the average crystallite size of the coating from the peak width at the half maximum of the crystal peaks[15].

$$d = k\lambda / (\beta_t \cos\theta) \quad (3)$$

where: d is the crystallite size; is the wavelength of the element used for the diffraction, is the peak width at the half maximum of the crystal peaks; and θ is the corresponding angle.

The microstrain was obtained using Equation 4[38]

$$\varepsilon = \beta_{hkl} \cos\theta / 4 \quad (4)$$

where: ε is the microstrain, is the full width at half maximum, and is the diffraction angle.

2.4. Deposition efficiency

Deposition efficiency of the galvanostatic deposition was evaluated through the current efficiency (% CE) using the following Equation 5:

$$(\%CE) = 100 \times \left(\frac{mr}{mc}\right) \quad (5)$$

where: *mr* is the mass of the Zn-Ni coating, and *mc* is the theoretical mass calculated using Equation 6[39]:

$$mc = \frac{t_i \,.M_i \,.i}{n_i \,.F.Ci} \quad (6)$$

where: t_i is the deposition time (second), M_i is the atomic mass of that element ($g.mol^{-1}$), i is the current of deposition (ampers), *Ci* is the weight fraction of metal, n_i is the number of electrons transferred and *F* is Faraday's constant.

The m_c can be related with the thickness of the coating following (Faraday's law) Equation 7:

$$t = m_c / d_{Zn-Ni}.S \quad (7)$$

where: t is the coating thickness, (μm); d_{Zn} is the Zn-Ni coating density ($g{\cdot}cm^{-3}$); S is the electrodeposition surface (cm^2).

2.5. Corrosion resistance

The effect of the addition of the CNC-Sif on the Zn-Ni coating corrosion resistance was evaluated in a 0.5 mol/L NaCl solution through mass loss measurements and electrochemical tests. Measurements were made at room temperature, around 25 °C, and all values were obtained in triplicate. The samples were immersed for 24 hours in the corrosive solution.

The cleaning of the surface of the Zn-Ni coating after immersion in an NaCl solution was performed with a solution of glycine (aminoacetic acid - $C_2H_5O_2N$) 1.36 mol/L at room temperature. The corrosion rate (CR) in mm per year was obtained from mass loss measurements, Equation 8[40]:

$$CR = \frac{K \times W}{A \times t \times D} \quad (8)$$

where: *K* is a constant (for *CR* mm/year, $K = 8.76 \times 10^4$); *W* is the mass loss (g); *A* is the exposed area (cm^2); *t* is the immersion time; (h) *D* is the density of the coating.

The electrochemical measurements, namely the potentiodynamic polarization and electrochemical impedance spectroscopy (EIS), were performed in a three-electrode cell using a saturated calomel electrode (SCE) as the reference electrode, and graphite as the counter electrode. These measurements were obtained with an AUTOLAB Potentiostatic & Galvanostatic model PGSTAT 100 instrument, using Autolab software NOVA 1.7. The potentiodynamic polarization curves were obtained at a scan rate of 10 $mV.s^{-1}$ in the anodic direction. The polarization resistance (Rp) values were obtained next to the corrosion potential (overpotential of 10 mV) from the inverse of the slope of a plot of the potential versus the current density. The samples were immersed in the corrosive solution for 3 min before being polarized.

The EIS measurements were performed at the corrosion potential over a frequency range of 100 kHz to 10 mHz, using a 10 mV amplitude of the sinusoidal voltage.

2.6. Microhardness

The Vickers microhardness measurements of coating were performed em um microdurometer (Model Shimazdu microdurometer – HMV series), carried out with a load of 100 g and time of load of 15 s. Measurements were made in triplicate.

3. Results and Discussion

3.1. Effect of the addition of CNC-Sif on the composition, morphology and structure of the Zn-Ni coating

Table 4 shows the effect of the CNC-Sif concentration in the bath on the Ni percentage in the coating. With the addition of 2% v/v, the Ni content in the coatings increases (from 8.7 wt.% to 9.5 wt.%). However, the effect of the nanocrystal concentration on the Ni content of coating shows no clear trend. Furthermore, the Ni content values obtained are within the margin of error.

Regarding the effect of ceramic particles on the composition of the Zn-Ni coating, this effect depends on the pH of the bath and on the type and concentration of the particles.

In alkaline deposition baths, it has been found that the addition of nanoparticles of ZrO_2, Al_2O_3, and SiC[18], as well as the addition of SiC micro-particles[41] does not affect the Ni percentage in the coating. A similar effect has been found in acid deposition baths regarding the addition of Al_2O_3 nanoparticles[42,43]. However, with the increase in the concentration of Al_2O_3 nanoparticles from 6 ml/L to 20 ml/L, there is a decrease in the Ni content in the coating. This effect was also observed[43] with the addition of SiC nanoparticles in the acid deposition bath, which resulted in a decrease in Ni concentration. The decrease in the concentration of Ni content with the addition of SiC nanoparticles is related to the increase in the hydrogen evolution reaction, HER, which results in the formation of the surface film of $Zn(OH)_2$, which can inhibit the reduction of cations of Ni[43]. Based on the effect of the addition of nanocrystals on current efficiency, as will be seen in Section 3.3, it is not possible to state that the presence of nanocrystals caused an increase in HER in the present work.

Table 4. Nickel percentages (%wt) in Zn-Ni deposits electroplated at different current densities from baths in the presence and absence CNC-Sif.

Nanocrystal concentration (% v/v)	Ni content (% wt)
0	8.7 ± 0.5
2	9.5 ± 0.5
3	9.6 ± 0.5
4	9.1 ± 0.5

Figure 1 shows the SEM images of the surface of the Zn-Ni coatings obtained from bath deposition without and with varying contents of CNC-Sif. In Figure 1 it can be seen that the coatings exhibit the characteristic nodular like morphology that is similar to the Zn-Ni coating obtained at 10 mA/cm^2 by Roventi et al.[18]. The effect of the addition of the CNC-Sif on the compactness of the coating is not noticeable, however, a greater agglomeration of the grains in the coatings obtained in the presence of 3%v/v and 4%v/v compared to the coating obtained in the presence of 2%v/v can be seen.

To analyze the effect of the CNC-Sif on the morphology more clearly, the coatings were analyzed using a confocal microscope to obtain images and observe roughness. Table 5 lists the roughness values of the Zn-Ni coatings in the absence and presence of different levels of the CNC-Sif.

Table 5. Roughness parameters of Zn-Ni coating in the absence and presence of different levels of CNC-Sif, where: Sa corresponds to the arithmetic mean of the absolute value of the surface departure above and below the mean plane within the sampling area, Sp to the height of the highest peak within the defined area, and Sv to the depth of the deepest valley within the defined area.

Nanocrystals (% v/v)	Sa (μm)	Sp (μm)	Sv(μm)
0	0.37 ± 0.06	3.93	3.14
2	0.21 ± 0.03	2.07	1.35
3	0.25 ± 0.04	2.37	1.57
4	0.29 ± 0.04	2.65	1.77

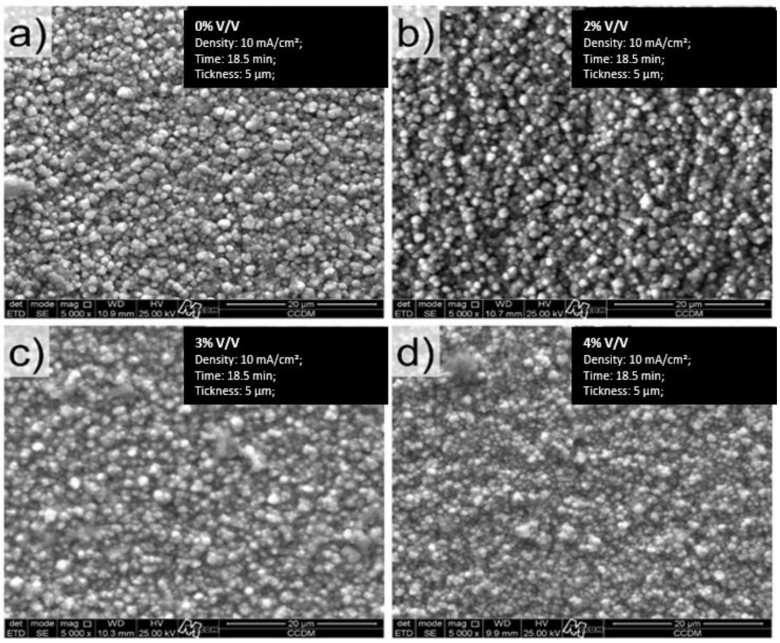

Figure 1. SEM image of surface of Zn-Ni coating electrodeposited from: a) bath without nanocrystals; b) bath containing 2%v/v of nanocrystals; c) bath containing 3%v/v of nanocrystals; d) bath containing 4%v/v of nanocrystals. Density: 10 mA/cm^2; Deposition time: 18.5 min; Tickness: 5 μm.

These results show that the addition of the nanocrystals reduces the roughness of the coating, and the lowest roughness value corresponds to the coating obtained in the presence of 2%v/v of the CNC-Sif.

The two-dimensional topographical images of the Zn-Ni coatings are shown in Figure 2. These images show that the coatings exhibit a sand dune-type morphology and that the addition of the nanocrystals changes the smoothness of the coating surface. With the addition of the nanocrystals, the width and height of the sand dune increase, and the coating surface becomes smoother and consequently less rough. This effect is more significant with the addition of 2% v/v of nanocrystals, indicating that there is an optimal concentration of nanocrystals at which the roughness is minimal.

It has been reported[44-46] that the effect of adding ceramic nanoparticles generally increases the roughness of metallic coatings obtained by electrodeposition. However, this effect depends on the amount and type of nanoparticle added, in addition to the coating composition. The addition of a small amount of graphene oxide (GO) nanoparticles decreases the roughness of the Ni coating obtained by electrodeposition but from the addition of 0.02 wt%, the roughness increases. It has also been found that the addition of SiC nanoparticles (20 g/L)[45] and of TiO_2-CeO_2 ceramic particles (2.5, 5, and 7.5 g/L)[46] increases the roughness of the Ni-P coating.

The effect of the addition of nanoparticles on the coating roughness is related to the introduction of defects due to the presence of the nanoparticles, the performance of the nanoparticle as a heterogeneous nucleation site, and the effect of the nanoparticle in inhibiting the diffusion of metallic cations in the solution during the electrodeposition process.

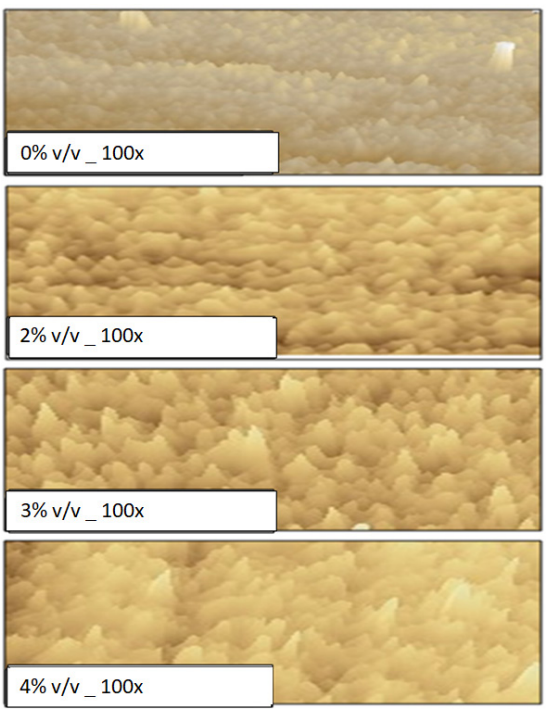

Figure 2. Two-dimensional topographical images from confocal microscopy of the Zn-Ni coatings obtained in the absence and presence of varying levels of CNC-Sif.

It is suggested that the presence of the nanoparticle introduces defects such as pores, making the coating less uniform. By acting as a nucleation site, the nanoparticles cause surface perturbation, which becomes more intense throughout the process, resulting in an increase in roughness. However, this effect depends on the distance between the nanoparticles, and the smaller the distance between them leads to a smoother deposit and, consequently, less roughness[45]. During the electrodeposition process, the presence of nanoparticles can inhibit the diffusion of metallic cations, thus limiting the free path for diffusion. This leads to the selective diffusion path of the metallic ion, resulting in the selective growth of the deposit and consequently the increase in roughness[44].

The factors that affect the roughness of the coating containing the nanoparticles depend on the level of agglomeration of the nanoparticles as a greater agglomeration favors the roughness of the coating. The increase in the agglomeration of nanoparticles results in a greater distance between the nucleation sites, which favors vertical growth to the detriment of horizontal growth, resulting in a more intense surface landscape and consequently greater roughness. A greater agglomeration of nanoparticles favors the diffusion hinderance of metallic cations and consequently the selective diffusion path of metallic ions. Furthermore, a greater agglomeration of nanoparticles may favor the occurrence of defects[44].

The decrease in the roughness of the Zn-Ni coating with the addition of the sisal fiber nanocrystals found in the present work indicates that the distribution of the nanocrystals was sufficiently homogeneous to avoid a more intense agglomeration that could increase the roughness. It is possible that the decrease in roughness caused by the addition of these nanocrystals is related to their performance as nucleation sites. With a sufficiently small distance between them this enables the formation of a less intense surface landscape and consequently a less rough surface. It is also possible that the nanocrystals, due to their small size, can fill the local defects (flaws, gaps, grooves) on the coating surface, making it less rough.

The increase in roughness with an increasing content of CNC-Sif beyond 2%v/v can be attributed to a greater agglomeration of nanocrystals. Although this agglomeration was not enough to increase the roughness in relation to the coating without the nanocrystals, it may have been enough to increase the distance between the crystals that act as nucleation sites and favor the selective diffusion path of the metallic ions.

Figure 3 shows the X-ray diffractogram pattern of the Zn-Ni coating obtained in the absence and presence of different concentrations of CNC-Sif. In this figure, the presence of fine diffraction peaks is observed, which is characteristic of the crystalline structure. In the diffractograms, the presence of the following phases is observed: the η phase, which corresponds to a solid solution of Ni in Zn (JCPDS card number 87-0712); the γ phase, which corresponds to a Ni_5Zn_{21} intermetallic compound (JCPDS card number 06-653); and the α phase, which corresponds to a solid solution of Zn in Ni (JCPDS card number 87-0713). The presence of Fe, peak (200), can also be observed and this occurs due to cracks in the coating, which results in the exposure of the steel substrate.

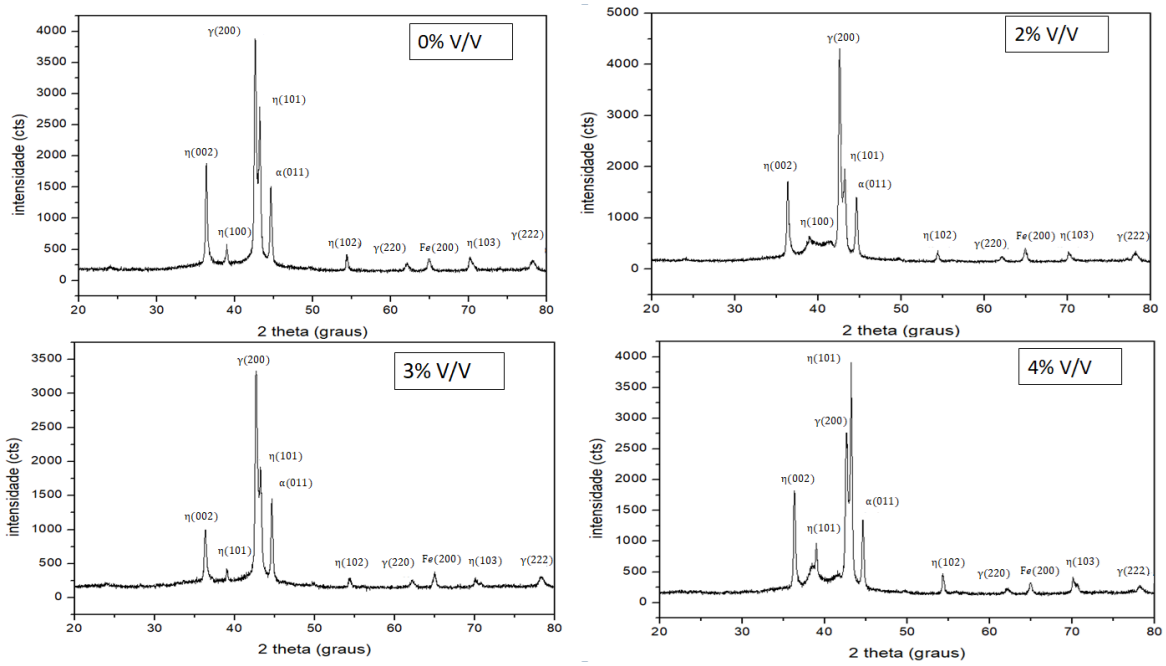

Figure 3. X-ray diffractogram pattern of the Zn-Ni coating obtained in the absence and presence of various concentrations of CNC-Sif.

The presence of phases in the Zn-Ni coating depends on the coating composition and deposition conditions. The η and γ phases are found in coatings with nickel contents from 5.0 to 14.0 wt.% obtained from an acid chloride bath[47], therefore, in a composition range which includes the coatings analyzed in the present work.

To investigate the effect of the addition of CNC-Sif on the crystallographic orientation of the Zn-Ni coating, the texture coefficient (Figure 4) was calculated for each peak of diffraction patterns. A higher texture coefficient, TC, for a given plane, indicates that the greater will be the preferred orientation of this plane in the coating. Figure 4 shows that the addition of 2.0% v/v and 3.0% v/v raises the TC corresponding to the γ(330) plane, and this effect is more significant with the addition of 2.0% v/v. In the Zn-Ni coating, the (330) plane, which corresponds to γ-Ni_2Zn_{11} phase[48], is more closely packed, thus the increase in the TC of the coatings content 2.0% v/v and 3.0% v/v leads to an increase in the coating packing density thus favoring increased corrosion resistance[15,48]. However, with the addition of 4%v/v, the TC corresponding to the (330) plane decreases in relation to the absence of CNC-Sif, while increasing the TC corresponding to (101) plane.

The crystallographic orientation of the Zn-Ni coating depends on the Ni content in the coating, so the increase in Ni content favors the crystallographic orientation in the (330) plane belonging to the γ phase[48]. However, the addition of CNC-Sif does not significantly affect the Ni content in the coating (Table 4). Furthermore, the coating obtained with the addition of 4%v/v of CNC-Sif has a TC for the plane (330) that is lower than that of the other coatings, although it has a higher Ni content than the other coatings, except for the coating obtained in the presence of 2%v/v.

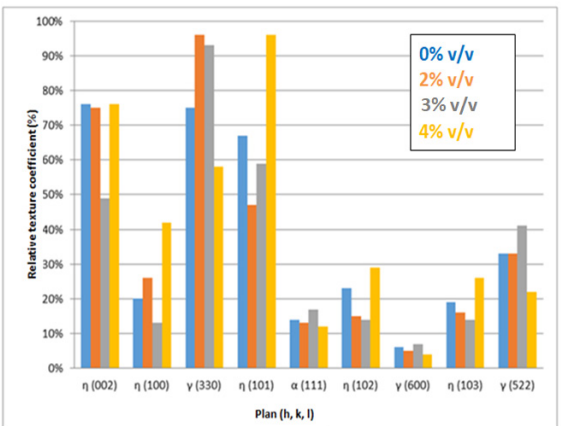

Figure 4. Texture coefficient of the Zn-Ni coating obtained in the absence and presence of varying concentrations of CNC-Sif.

The increase in intensity of the γ phase with (330) plane orientation in an Zn-Ni coating due to the addition of nanometer-sized particles has also been observed with the incorporation of ceramic nanoparticles such as Al_2O_3[15] and TiO_2[48]. However, it is unclear how this effect occurs.

It is possible that the effect of the addition of the CNC-Sif in the presence of the crystallographic planes is related to the fact that the nanocrystals act as a heterogeneous nucleation site. The growth of the metallic deposit during the deposition process tends to occur preferentially in the planes with lower free energy[49], and the nucleation from the nanocrystals favored the growth of the deposit in the plane (330). However, in the coating obtained with the addition of 4%v/v of nanocrystals, a greater agglomeration of the

nanocrystals may occur, resulting in a greater separation of the nanocrystals that act as nucleation sites, which may have favored the growth of crystallites parallel to the plane (101).

From the X-Ray diffraction patterns (Figure 3), the sizes of the crystallites, considering the average of the three highest intensity peaks, and the microstrain present in the Zn-Ni obtained in the absence and in the presence of the nanocrystals were determined. These results, which are listed in Table 6, show that the effect of the addition of these nanocrystals on the crystallite size depends on the concentration of the crystallite added in the deposition bath. The addition of 2% v/v and 3% v/v of CNC-Sif results in a reduction in the size of the crystallites. However, the addition of 4% v/v causes the crystallites to increase in size.

Depending on the amount and type of nanoparticles, the incorporation of ceramic nanoparticles in the Zn-Ni coating can cause either a decrease or an increase in the size of the crystallites. It has been found that with the incorporation of Al_2O_3[15], SiO_2[50], and WC[51], the nanoparticles reduce the size of the Zn-Ni coating crystallites. However, Roventi et al.[18] found that the incorporation of ZnO_2 and Al_2O_3 nanoparticles increases the crystallite size, while the addition of SiC nanoparticles does not appreciably affect the crystallite size.

The decrease in crystallite size caused by the addition of the nanoparticles is related to the role of the nanoparticle as a site of heterogenous nucleation, and to the effect of the nanoparticle on the atomic diffusion during the deposition process. With the increase in the number of nucleation sites, and consequently in the nucleation rate, there is a decrease in the distance between them, which restricts the growth of crystallites, thus resulting in their refining[50,51]. On the other hand, the presence of nanoparticles inhibits the surface diffusion of atoms toward growing centers, which inhibits crystallite growth[52]. It has also been suggested that the nanoparticle acts as a protuberance at the metallic layer/substrate interface, which results in an increase in current density and nucleation rate[51].

The fact that ceramic nanoparticles as well as the sisal nanocrystals analyzed in the present work have a contradictory effect on refining the crystallites is probably related to the distribution of these particles during the deposition process. A more uniform distribution of nanocrystals results in a smaller distance between them, and therefore between the nucleation sites, which favors the refining of crystallites. However, from a certain concentration of nanocrystals, the level of agglomeration of the nanocrystals increases with increasing concentration, resulting in a greater distance between them, which has a less effective effect on inhibiting the size of the crystallites. This behavior may be related to the lower crystallite refining caused by the presence of 3%v/v of CNC-Sif in relation to the addition of 2%v/v. A higher concentration of nanocrystals, as observed with the addition of 4%v/v, probably resulted in a level of agglomeration of the nanocrystals that caused a distance between them that did not allow the refining of crystallites to occur, despite favoring their growth.

In relation to microstrain, the results in Table 6 show that this parameter has an inverse behavior in relation to the size of the crystallites, with an increase in the microstrain as the grain size decreases. A similar behavior was found with the incorporation of silica nanoparticles and Mesoporous-silica (MPS) in the Zn coating[53], with the incorporation of a carbon nanotube in the Ni coating[54], and with the incorporation of Y_2O_3 nanoparticles in the Ni- W coating[55].

The increase in the microstrain of the metallic coating with the incorporation of the nanoparticle is related to the inconsistency between the nanoparticle and the metallic matrix[54]. The addition of 2%v/v and 3%v/v of CNC-Sif promotes a mismatch between the nanocrystals and the Zn-Ni matrix, which causes tension between these phases and consequently increases the microstrain. As with the size of the crystallites, the presence of the nanocrystals in the microstrain is also related to the distribution of the nanocrystal coating. With the increase in the content of the nanocrystals from a certain value, the agglomeration of nanocrystals is favored, which reduces the amount of nanocrystals per volume to a level that leads to a decrease in the level of strain introduced by them. This behavior is related to the decrease in microstrain from the addition of 2% v/v of nanocrystals. This has also been observed with the incorporation of carbon nanotubes in the Ni coating[54] and Y_2O_3 nanoparticles in the Ni-W coating[55]

The increase in microstrain can cause cracking in the coating, resulting in the deterioration of the corrosion resistance[56]. However, the SEM photomicrographs (Figure 1) show that the increase in microstrain of the coating in the coatings containing 2% v/v and 3% v/v CNC-Sif was not sufficient to cause cracking in these samples.

3.2. Current efficiency

Figure 5 shows the effect of adding CNC-Sif on the current efficiency of a Zn-Ni coating. The results indicate that the addition of 2% v/v of the nanocrystals in the deposition bath increases the deposition efficiency of the Zn-Ni coating. However, as the nanocrystal content increases from this concentration, the current efficiency tends to decrease, and it is observed that the values corresponding to the addition of 4% v/v is within the margin of error of the current efficiency corresponding to the absence of these nanocrystals.

Some studies have found an increase in the current efficiency of metallic coatings with the addition of ceramic nanoparticles such as Al_2O_3 in Cr[57], SiC in Ni[58], and ZnO in Ni[59].

Table 6. Crystallite size and microstrain values of Zn-Ni coating obtained in the absence and presence of varying concentrations of CNC-Sif.

Nanocrystal concentration (%v/v)	Crystallite size (nm)	Microstrain <ε>
0	57.4	0.00067
2	48.0	0.00081
3	51.7	0.00078
4	64.8	0.00057

To explain the increase in current efficiency due to the addition of ceramic nanoparticles, it has been proposed[49] that the transport of metallic ions towards the cathode surface is facilitated by the formation of a film of these ions around the nanoparticles, which makes reduction faster.

The effect of the addition of an additive on the deposition efficiency of metallic coatings is often related to viscosity and hydrogen evolution. With the increase in the viscosity of the deposition bath, the mass transport of metallic cations to the cathode/solution interface is inhibited, resulting in a decrease in the deposition current of metallic cations and, consequently, in the current efficiency[60]. However, as can be seen from Table 3, the addition of CNC-Sif to the deposition bath increases the conductivity of the bath, which indicates that the viscosity is not altered by the presence of the nanocrystals. The increase in hydrogen evolution, as this is a concurrent reaction of the reduction reaction of metallic cations, tends to decrease the deposition efficiency. However, the results indicate that the addition of the nanocrystals does not cause a sufficient increase in hydrogen evolution to decrease the current efficiency.

It is possible that the effect of the addition of CNC-SiF on the current efficiency is related to the morphology of the coating. The hydrogen evolution reaction and consequently the decrease in current efficiency is favored by the presence of defects on the coating surface, as the defects act as hydrogen adsorption sites[61]. As seen in Table 5, the addition of CNC-Sif, mainly at 2% v/v, reduces the roughness of the coating, which indicates a more compact surface with fewer defects, which can result in less hydrogen evolution, and consequently higher current efficiency. The decrease in roughness with increasing nanocrystal content from 2% v/v may be related to the increase in current efficiency due to this content. It is also possible that the increase in current efficiency is related to the performance of the nanocrystal as a heterogeneous nucleation site. As seen in item 3.1, the decrease in crystallite size caused by the addition of the nanocrystals indicates the role of the nanocrystals as nucleation sites. The decrease in current efficiency from the 2% v/v content may also be related to the increase in the agglomeration level of the nanocrystals, which results in a decrease in the number of nucleation sites.

3.3. Effect of the addition of sisal nanocrystals on the corrosion resistance of the Zn-Ni coating

The effect of the addition of the CNC-Sif on the corrosion resistance of Zn-Ni coating was investigated through mass loss tests and electrochemical tests. These tests include obtaining the corrosion potential, E_{corr}, and the polarization resistance, R_p, through the potentiodynamic polarization curve, and electrochemical impedance tests.

Figure 6 shows the values of the corrosion rate obtained from the mass loss tests carried out after 24 hours of sample immersion in 0.5 M NaCl solution. The results show that the addition of the nanocrystals up to a content of 3%v/v decreases the corrosion rate of the coating, and this is lower for a content of 2%v/v. The addition of 1% v/v of CNC-Sif does not significantly change the corrosion rate of the coating.

The potentiodynamic polarization curves, Tafel curves, of the coating obtained in the absence and presence of varying levels of CNC-Sif contents are represented in Figure 7.

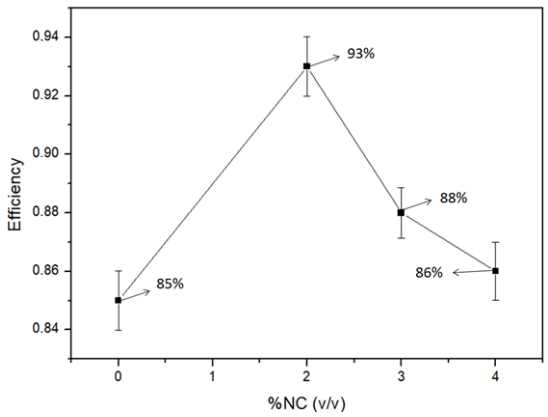

Figure 5. Current efficiency of the electrodeposition process of a Zn-Ni coating obtained in the absence and presence of varying amounts of CNC-Sif.

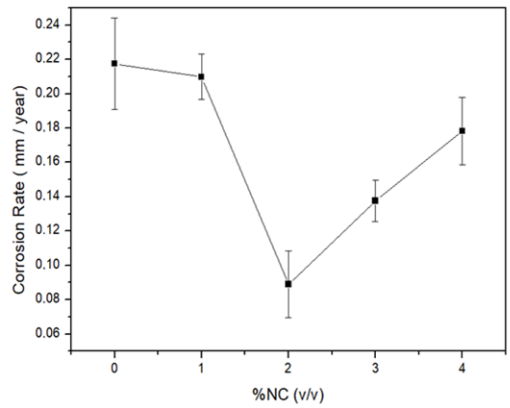

Figure 6. Corrosion rate obtained from mass loss tests of Zn-Ni coatings obtained in the absence and presence of varying levels of CNC-Sif.

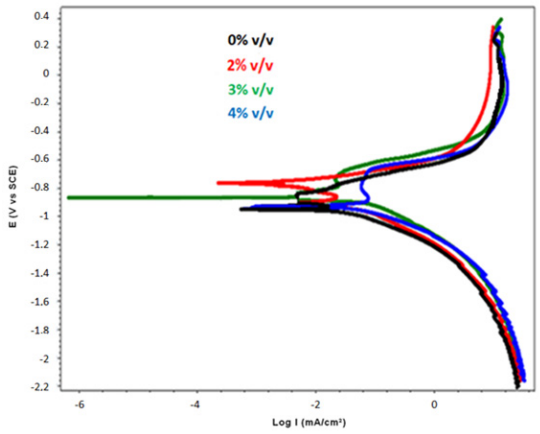

Figure 7. Potentiodynamic polarization curves in the 0.5 M NaCl solution of the Zn-Ni coatings obtained in the presence of varying concentrations of CNC-Sif added to the bath deposition. The curves were obtained at a scanning rate of 10 mV/s.

The corrosion potentials, E_{cor}, obtained from these curves are listed in Table 7. These results show that samples containing nanocrystals have a higher E_{cor}, which indicates that they tend to present a higher corrosion resistance, and this is higher for the coating obtained in the presence of 2% v/v of CNC-Sif. However, a higher E_{cor} does not necessarily indicate a lower corrosion rate. An important limitation of using E_{cor} to evaluate the corrosion resistance is that the effect of the presence of the corrosion product on the corrosion rate is not taken into consideration[62].

Figure 7 shows that in the anodic region from the potential around -0.4 V vs ECS the current density presents a small variation, indicating behavior passivation. This is also observed in the Zn potentiodynamic polarization curve in the 0.5 M NaCl solution[63]. The curve corresponding to the addition of 2% v/v of CNC-Sif displays the lower current density in this region compared to the other curves. This indicates a greater protective capacity of the passive film of the coating containing this concentration of nanocrystals, which should favor the corrosion resistance of this deposit in relation to the others. However, it is not possible to clearly distinguish the current density in the passive film forming region. This difficulty in distinguishing the corrosion resistance of coatings using qualitative analysis of the potentiodynamic polarization curves was also observed in the results obtained by Close et al.[63]. These authors investigated the effect of the addition of the additive (Hydroxybenzaldehyde (4-HB) and Ammonium Thiocyanate (NH4SCN)) on the corrosion resistance of a Zn-Mn coating in NaCl solution, by linear polarization resistance. Their results indicate that although the addition of the additive decreases the corrosion rate of the coating, it is not possible to distinguish the potentiodynamic polarization curves of these coatings in the anodic region.

It is possible that the addition of 2% v/v of CNC-Sif acted as a support for the formation of corrosion products that act as a passive film, thus favoring the formation of these products. However, this effect is not clear in relation to the other concentrations analyzed. It has been found that ceramic nanoparticles such as Si2O2 act as a support for the formation of zinc hydroxide chloride (Zn5(OH)8Cl2H2O) which acts as a passive film favoring an increase in the corrosion resistance of Zn coating in an NaCl solution. However, for the formation of zinc hydroxide chloride, the coating should remain immersed in the solution for a minimum time[64].

In a future work, the effect of CNC-Sif on the formation of corrosion products in the Zn-Ni coating will be investigated using XPS and X-Ray diffraction after the coating has remained immersed in the NaCl solution for different periods. Furthermore, there are plans to investigate how this affects the corrosion rate of the coating.

Figure 8 shows the values of polarization resistance, R_p, obtained from the potentiodynamic polarization curves of potential vs current density. Considering that a higher value of R_p indicates a greater resistance to corrosion, Figure 8 shows that the addition of the CNC-Sif decreases the corrosion rate of the coating, with the sample containing 2%v/v of nanocrystals performing the best.

The results from electrochemical impedance (EIS) are shown in Figure 9 and Figure 10, which refer to Nyquist and Bode impedance modulus diagrams (log |Z|=f (log ω)), respectively.

Table 7. Corrosion potential, E_{cor}, in 0.5 M NaCl solution of Zn-Ni coating obtained in the absence and in the presence of varying levels of CNC-Sif.

NC (% v/v)	E_{cor} (mv)
0	-1020.872
2	-776.780
3	-860.138
4	-912.097

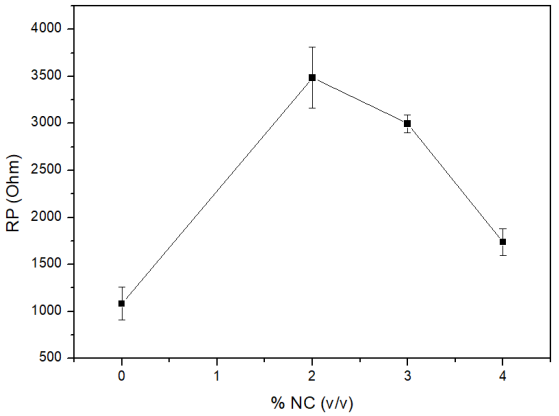

Figure 8. Polarization resistance of Zn-Ni coating obtained in the absence and presence of different concentrations of CNC-Sif.

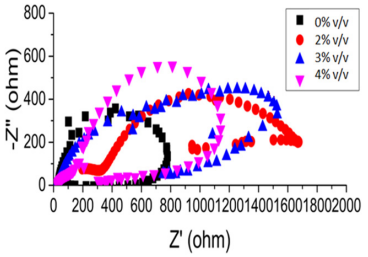

Figure 9. Nyquist plot in 0.5M NaCl solution for Zn-Ni coatings obtained in the absence and presence of varying concentrations of CNC-Sif.

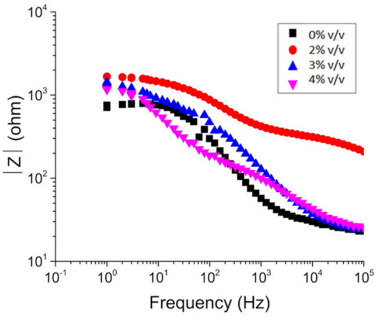

Figure 10. Bode plot in 0.5M NaCl solution for Zn-Ni coatings obtained in the absence and presence of varying concentrations of CNC-Sif.

The equivalent circuit model used in the treatment of experimental data is shown in Figure 11. Parameters Rccc and Qcc refer to the resistance and pseudo capacitance of the coating, respectively. Rct and Qdl refer to the charge transfer resistance and the double layer pseudo capacitance, respectively, and Rs corresponds to the solution resistance[65].

As seen in Figure 9, the Nyquist diagram of all the coatings shows a depressed semicircle shape. Considering that a larger diameter of the semicircle indicates a greater resistance to corrosion, Figure 9 shows that the coating containing 2% v/v of CNC-Sif is the one with the greatest corrosion resistance, while the lowest one was seen in the coating without the addition of the CNC-Sif.

Like the Nyquist diagram, the Bode impedance modulus diagram (Figure 10) can also be used to evaluate the corrosion resistance of the coating. In the high frequency region, above 2000 Hz, the log |Z| is smaller and tends to remain constant. This indicates a resistive response, which in turn corresponds to the solution resistance (Rs). In the intermediate frequency range, the |Z| decreases with increasing frequency. On the other hand, in the low frequency region, with values lower than 1Hz, the impedance behavior is associated with the polarization resistance and the higher impedance modulus indicates a higher polarization resistance and consequently greater corrosion resistance[66]. Therefore, Figure 10 also indicates that addition of the CNC-Sif increases the corrosion resistance of the coating and this effect is more significant in the presence of 2% v/v. The EIS results, as well as the results obtained from the polarization curves and the mass loss tests show that the addition of the CNC-Sif increases the corrosion resistance of the Zn-Ni coating. The optimal concentration, among the analyzed concentrations, is 2% v/v, at which the corrosion resistance is maximum. As can be seen in Figure 6, the results regarding the corrosion rate of the sample obtained in the presence of 4% v/v of nanocrystals are in the same margin of error as the corrosion rate corresponding to the sample obtained in the absence of the nanocrystals. However, electrochemical tests show that the addition of 4% v/v of the CNC-Sif increases the corrosion resistance of the Zn-Ni coating. This inconsistency may be due to a limitation of the mass loss measurements. This is related to the difficulty of completely removing the corrosion products from the samples after immersion in the aggressive solution.

Based on the results listed in Table 4, it is not possible to state that the decrease in the corrosion rate of the Zn-Ni coating is related to the increase in the Ni content in the coating. Although the addition of 2% v/v of CNC-Sif does result in a small increase in the Ni content, the addition of 3% v/v does not result in an increase in the Ni content and despite this, there is an increase in corrosion resistance in relation to the nanocrystal-free coating. As with ceramic nanoparticles, as seen in the introduction, the increase in the Zn-Ni corrosion resistance due to the addition of the CNC-Sif is probably related to the change in the morphology and structure of the coating caused by the incorporation of the nanocrystals. Therefore, investigations into the effect of the addition of CNC-Sif on roughness, texture coefficient, crystallite size, and microstrain help to understand the effect of this addition on the corrosion rate of the Zn-Ni coating.

Given their nanometric dimensions, the nanocrystals are small enough to fill defects, such as gaps and pores, making the coating surface smoother. This effect decreases the surface contact area with the corrosive solution, thus improving the corrosion resistance of the coating. Furthermore, the reduction in defects that could act as active corrosion sites also favors the increase in corrosion resistance. The smoothness of the surface can be evaluated through the measurement of roughness, with a lower roughness indicating a smoother surface, which favors an increase in corrosion resistance. Therefore, the decrease in roughness caused by the addition of the nanocrystals (Figure 2) may have contributed to the increase in the corrosion resistance of the Zn-Ni coating, and the sample with the lowest roughness is the one with the highest corrosion resistance. However, it has been found[36,46] that the addition of nanoparticles can lead to increased corrosion resistance, despite the fact that this addition results in increased roughness. This therefore indicates that the increase in the corrosion resistance of the metallic coating due to the addition of nanoparticles is also related to other factors.

The change in the presence of the crystallographic planes can affect the behavior of the metallic coating in relation to corrosion. In a more closely packed plane, the atoms are closer to each other, thus increasing the binding energy, favoring the corrosion resistance of the coating[48]. The increase in the presence of the γ(330) plane with the addition of 2% v/v and 3%v/v of CNC-Sif (Figure 3 and Figure 4) therefore favors an decrease in the corrosion rate of the coating, considering that this plane exhibits a more closely packed surface. The higher corrosion resistance of the coating containing 2% v/v CNC-Sif is consistent with the fact that it has a higher TC. The increase in the presence of the η(101) plane to the detriment of the γ(330) plane with the addition of 4% v/v may have contributed to the lower corrosion resistance of the coating compared to the samples containing 2% v/v and 3% v/v. However, the fact that the coating containing 4% v/v exhibits a superior corrosion resistance than the coating without CNC-Sif, despite the fact that this coating has a greater presence of the γ(330) plane, indicates that the presence of the crystallographic plane is not the factor determining the effect of the nanocrystals on the corrosion resistance of the Zn-Ni coating.

The refining of metallic coating grains is often related to increased corrosion resistance of a metallic coating[67,68].

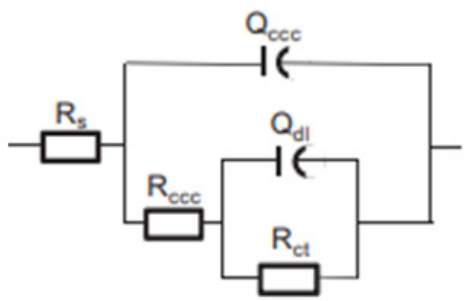

Figure 11. Equivalent electrical circuits used for the analysis of impedance spectra.

Therefore, considering that the decrease in crystallite size indicates the occurrence of grain refining, the results obtained in the present work are consistent with the fact that the addition of the nanocrystals causes both the refining of crystallites and an increase in the corrosion resistance of the coating. Even the coating containing 2% v/v of CNC-Sif, which is the one with the highest corrosion resistance, is the one with the highest grain refinement. The effect of grain refining in increasing the corrosion resistance of the coating is attributed to a greater dispersion of the corrosion current, which results in a lower occurrence of localized corrosion[67]. However, it is not clear how this current density dispersion occurs due to grain refining.

Microstrain can affect the corrosion rate of the coating because the increase in microstrain can cause cracking which results in the deterioration of the coating's corrosion resistance. As observed in Table 6, the addition of the CNC-Sif increases the microstrain of the coating, however, this increase was not enough to affect the corrosion rate of the coating, and the coating containing 2% v/v, which exhibits a higher microstrain, is the one that presents a greater resistance to corrosion.

In addition to the effect of the presence of the nanocrystals on the microstructure and morphology of the coating, the increase in corrosion resistance may be related to other effects as mentioned earlier (see Introduction). It is possible that the incorporation of the nanocrystals in the coating results in a decrease in the active surface in contact with the corrosive solution, thus increasing the corrosion resistance of the coating[15]. As suggested in relation to the incorporation of graphene oxide[69] and silica nanoparticles[70], it is also possible that the incorporation of nanocrystals hinders the diffusion of oxygen, thus inhibiting the reduction reaction with the consequent increase in corrosion resistance. By presenting a low level of electrical conductivity, it is also possible that nanocrystals, when uniformly dispersed in the coating, cause an increase in the resistance to current flow, in addition to promoting the distract of this current flow[44,71].

As mentioned in the Introduction regarding TiO2 and CeO2 nanoparticulates incorporated in the Ni-P coating, it is also possible that the presence of nanocrystals favors uniform corrosion at the expense of localized corrosion, thus making the coating more resistant to corrosion. This effect is attributed to the introduction of corrosion microcells with the nanoparticle acting as the cathode and the Zn-Ni matrix as the anode, which results in a more uniform distribution of corrosion[72].

The effect of the nanocrystal concentration on the corrosion resistance of the Zn-Ni coating is probably related to the distribution of the nanocrystals in the coating because, as seen in item 3.2, this distribution affects the microstructure and morphology of the coating. With the increase in the CNC-Sif content above 2% v/v, which should result in a less uniform distribution and favor the agglomeration of the nanocrystals, there is an increase in roughness, in the size of the crystallites, and a decrease in the presence of the γ(330) plane, all of which can collaborate to reduce the corrosion resistance of the coating. In addition, a greater agglomeration of the nanocrystals decreases the intensity of the nanocrystal binding with the metallic matrix, which can cause the nanocrystals to be removed from the matrix, resulting in the formation of defects such as gaps and pores. These defects act as active corrosion sites favoring a decrease in the corrosion resistance of the coating[73].

The distribution of the nanocrystals should also affect their efficiency in acting as a protective barrier against the action of the corrosive medium. As the agglomeration of nanocrystals occurs with increasing concentration, the distance between them increases, thus impairing the inhibitory action that they exert in relation to the diffusion of ions and the electric current. Furthermore, the increase in the size of the nanocrystals, resulting from the agglomeration, restricts their ability to fill the defects present in the coating, and therefore, to make the coating more compact and uniform.

In the present work, the effects resulting from the increase in the concentration of CNC-Sif from 2% v/v, which resulted in a decrease in corrosion resistance, were not sufficient to reduce the corrosion resistance of the Zn-Ni coating in relation to the absence of the additive. However, the results obtained show that there is an optimal content of additive, and that for higher levels it is possible that the addition of the nanocrystals results in the deterioration of the corrosion resistance of the coating. It can also be seen that the mechanisms through which the addition of the nanocrystals affects the corrosion resistance of the Zn-Ni coating are complex and it is not possible to determine what the predominant mechanism might be.

Ni is added to the Zn-Ni alloy in order to decrease the alloy's corrosion rate, but it has a higher cost than Zn. Therefore, increasing the corrosion resistance of Zn-Ni through the addition of a relatively low cost additive such as CNC-Sif is important because it reduces the Ni content required in the alloy. In a future work, the effect of the addition of CNC-Sif on the corrosion resistance of Zn-Ni coatings containing different concentrations of Ni will be analyzed in order to determine how much the concentration of Ni in the coating can be reduced with the addition of CNC-Sif.

It is also important to mention that in nanocomposites containing ceramic nanoparticles, surfactants are often added to minimize the agglomeration of the nanoparticles and consequently increase the corrosion resistance of the coating. For example, the surfactant cetyl trimethyl ammonium bromide is added to the deposition bath of the Zn-Ni coating to minimize the agglomeration of TiO2 nanoparticles[74]. Therefore, in a future work, the effect of the presence of a surfactant on the agglomeration of the CNC-Sif will be analyzed.

3.4. Effect of the addition of sisal nanocrystals on the microhardness of the Zn-Ni coating

The microhardness values of the Zn-Ni coatings in the absence and presence of different levels of the CNC-Sif are shown in Figure 12. These results show that the addition of the nanocrystals increases the microhardness of the coating, and the highest microhardness value corresponds to the coating obtained in the presence of 2%v/v of the CNC-Sif. Although the behavior of the coating in relation to wear resistance must be analyzed through specific tests, the increase in hardness indicates a tendency to increase wear resistance which is an important characteristic in the application of the coating.

According with Praveen and Venkatesha[74] an increase of around 9% in microhardness is a significant improvement in applications of the coatings at an industrial scale. It is observed in Figure 12 that the addition of 2%v/v of the CNC-Sif results in an increase of at least 20% in the microhardness of coating.

The increase in the microhardness of coating due to the addition of nanoparticles has also been observed with the addition of ceramic nanoparticles such as SiO2 and TiO2[75-78]. This effect is mainly attributed to grain refining, dispersion-strengthening[53] and, the high hardness of the nanoparticles that inhibits the deformation of the coating matrix (particle-strengthening)[75]. Due to the low hardness of the natural polymer, the addition of CNC-Sif should collaborate to reduce the microhardness of coating, however the results indicate that the effects of grain refining and dispersion-strengthening prevail.

As observed in Table 6, the addition of 2% v/v and 3% v/v of the CNC-Sif decreases the size of the crystallites, which may indicate a grain refining. Therefore, it is possible that the increase in microhardness with the addition of these nanocrystal concentrations is related to the decrease in grain size. Grain refining implies an increase in the area of the grain boundary, which hinders the movement of dislocations with the consequent increase in microhardness. Dispersion-strengthening is an important mechanism in increasing the microhardness of the coating due to the presence of nanoparticles[76]. It is possible that due to their small size, the CNC-Sif nanocrystal interact with the dislocations, resulting in increased microhardness.

The lower microhardness of coating with the addition of 3% v/v and 4%v/v compared to the addition of 2% v/v may be related to the increase in the agglomeration level of the nanocrystals, which results in a decrease in the number of nancrystal per coating volume. Therefore, with the increase in nanocrystal concentrations from 2% v/v, the effect of dispersion-strengthening and grain refining on the increase in microhardness becomes less intense. The microhardness results are consistent with results referring to current efficiency and corrosion resistance, which show that these properties are better with the addition of 2% v/v and deteriorate with increasing CNC-Sif concentration, probably due to the agglomeration of these nanocrystals.

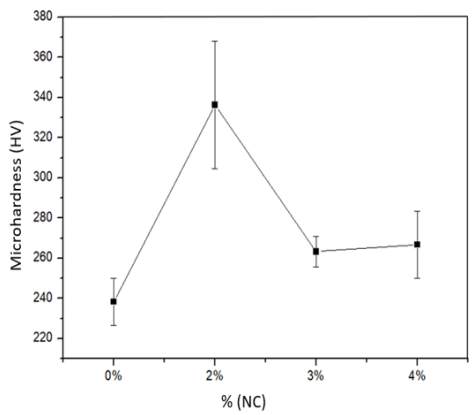

Figure 12. Microhardness values of the Zn-Ni coatings in the absence and presence of different levels of the CNC-Sif.

In prior work it was found that the addition of cotton nanocrystal[9] and soybean nanocrystal[8] to the Zn coating reduces the hardness of the coating. This effect is attributed to the presence of weak interfacial bonding strength between the nanocrystals and the matrix collaborating to decrease the hardness of the coating. However, the results obtained in relation to the effect of CNC-Sif on the microhardness of Zn-Ni coating in the present work, show that the interfacial bonding strength between the nanocrystals and the matrix depends on the nanocrystal.

4. Conclusion

Zn-Ni coatings containing various concentrations (2% v/v, 3% v/v, and 4% v/v) of cellulose nanocrystals obtained from sisal fiber were investigated.

The addition of the CNC-Sif in the deposition bath affects the morphology and structure of the Zn-Ni coating, and this effect is more pronounced with the addition of 2% v/v of nanocrystals.

There is a decrease in roughness, and with the exception of the concentration of 4% v/v, there is a decrease in the size of the crystallites and an increase in the microstrain, favoring the presence of γ(330) planes.

The current efficiency is increased with the addition of the sisal nanocrystals up to a concentration of 3% v/v, and this effect is more significant with the addition of 2% v/v.

The corrosion resistance of the Zn-Ni coating is increased with the addition of CNC-Sif in the deposition bath. It was found that there is an optimal content of nanocrystals, namely 2% v/v, at which corrosion resistance is maximum. This is related to the effect of the nanocrystals on the morphology and structure of the Zn-Ni coating.

The addition of the nanocrystals increases the microhardness of the coating, and the highest microhardness value corresponds to the coating obtained in the presence of 2%v/v of the CNC-Sif

5. Acknowledgments

This project was financially supported by the Fundação de Amparo à Pesquisa do Estado da Bahia

6. References

1. Zhang XG. Galvanic corrosion of zinc and its alloys. J Electrochem Soc. 1996;143:1472-85.
2. Wasekar NP, Jyothirmayi A, Hebalkar N, Sundararajan G. Influence of pulsed current on the aqueous corrosion resistance of electrodeposited zinc. Surf Coat Tech. 2015;272:373-9.
3. Polyakov NA, Botryakova IG, Glukhov VG, Red'kina GV, Kuznetsov YI. Formation and anticorrosion properties of superhydrophobic zinc coatings on steel. Chem Eng J. 2021;421:27775.
4. Azar MMK, Gugtapeh HS, Rezaei M. Evaluation of corrosion protection performance of electroplated zinc and zinc-graphene oxide nanocomposite coatings in air saturated 3.5 wt.% NaCl solution. Colloids Surf A Physicochem Eng Asp. 2020;601:125051.
5. Sajjadnejad M, Mozafari A, Omidvar H, Javanbakht M. Preparation and corrosion resistance of pulse electrodeposited Zn and Zn–SiC nanocomposite coatings. Appl Surf Sci. 2014;300:1-7.
6. Sajjadnejad M, Ghorbani M, Afshar A. Microstructure-corrosion resistance relationship of direct and pulse current electrodeposited Zn-TiO2 nanocomposite coatings. Ceram Int. 2015;41:217-24.

7. Fayomi OSI, Popoola AOI, Olorunniwo OE. Structural and properties of Zn-Al2O3-SiC nano-composite coatings by direct electrolytic process. Int J Adv Manuf Technol. 2016;87:389-98.
8. Lopes CS, Rovere CAD, Rigoli IC, Rocha CLF, Souza CAC. Electrodeposited Zn-soybean nanocrystal composite coatings: an effective strategy to produce cheaper and corrosion resistant Zn composite coatings. J Mater Res Technol. 2022;20:1378-90.
9. Lopes CS, Rigoli IC, Rovere CAD, Rocha CLF, Souza CAC. Electrodeposition and the properties of a Zn-Cotton nanocrystal composite coating. Electrodeposition and the properties of a Zn-Cotton nanocrystal composite coating. J Mater Res Technol. 2022;17:852-65.
10. Arrighi C, Savall C, Cohendoz S, Grosseau-Poussard JL, Baissac L, Olivier MG, et al. Optimization of the morphology, structure and properties of high iron content Zn–Fe coatings by pulse electrodeposition. Mater Chem Phys. 2021;263:124366.
11. Lotfi N, Aliofkhazraei M, Rahmani H, Darband GB. Zinc–nickel alloy electrodeposition: Characterization, properties, multilayers and composites. Prot Met Phys Chem Surf. 2018;54:1102-40.
12. Kumar CMP, Lakshmikanthan A, Chandrashekarappa MPG, Pimenov DY, Giasin K. Electrodeposition based preparation of Zn–Ni Alloy and Zn–Ni–WC nano-composite coatings for corrosion-resistant applications. Coatings. 2021;11(6):712.
13. Kumar CMP, Venkatesha TV, Vathsala K, Nayana KO. Electrodeposition and corrosion behavior of Zn–Ni and Zn–Ni–Fe2O3 coatings. J Coat Technol Res. 2012;9:71-7.
14. Praveen BM, Venkatesha TV. Electrodeposition and corrosion resistance properties of Zn-Ni/TiO2 nano composite coatings. Int J Electrochem. 2011;2011:261407.
15. Blejan D, Muresan LM. Corrosion behavior of Zn-Ni-Al2O3 nanocomposite coatings obtained by electrodeposition from alkaline electrolytes. Materials and Corrosion. 2012;64:433-8.
16. Ullal Y, Chitharanjan AH. Corrosion protection of electrodeposited multilayer nanocomposite Zn-Ni-SiO2 coatings. Surg Eng Appl Electrochem. 2013;49:161-7.
17. Exbrayat L, Rébéré C, Eyame CRN, Steyer P, Creus PJ. Corrosion behavior in saline solution of pulsed-electrodeposited zinc-nickel-cerio nanocomposite coatings. Materials and Corrosion. 2017;73:1-14.
18. Roventi G, Giuliani G, Pisani M, Bellezze T. Electrodeposition of Zn-Ni-ZrO2, Zn-Ni-Al2O3 and Zn-Ni-SiC nanocomposite coatings from an alkaline bath. Int J Electrochem. 2013;12:663-78.
19. Roventi G, Bellezze T, Fratesi R. Electrodeposition of Zn–SiC nanocomposite coatings. J Appl Electrochem. 2013;43:839-46.
20. Raquez JM, Habibi Y, Murariu M, Dubois P. Polylactide (PLA)-based nanocomposites. Prog Polym Sci. 2013;38(10-11):1504-42.
21. Besbes I, Vilar MR, Boufi S. Nanofibrillated cellulose from Alfa, Eucalyptus and Pine fibres: preparation, characteristics and reinforcing potential. Carbohydr Polym. 2011;86:1198-206.
22. Eichhorn SJ. Cellulose nanowhiskers: promising materials for advanced applications. Soft Matter. 2011;7(2):303-15.
23. George J, Sabapathi SN. Cellulose nanocrystals: synthesis, functional properties, and applications. Nanotechnol Sci Appl. 2015;8:45-54.
24. Kumar R, Chauhan S. Cellulose nanocrystals based delivery vehicles for anticancer agent curcumin. Int J Biol Macromol. 2022;22:842-64.
25. Filho AJFS, Menezes A, Magalhaes DP, Peireira-da-Silva MA, Carvalho AJF. Preparação e caracterização de nanocristais de celulose a partir de polpa de eucalipto e sisal. In: 10 CBPOL; 2009. Proceedings. São Carlos: Associação Brasileira de Polímeros; 2009. p. 1-9.
26. Parize DDS, Oliveira JE, Williams T, Wood D, Avena-Bustillos RJ, Klamczynski AP, et al. Solution blow spun nanocomposites of poly(lactic acid)/cellulose nanocrystals from Eucalyptus kraft pulp. Carbohydr Polym. 2017;174:923-32.
27. Flauzino WP No, Silvério HA, Dantas NO, Pasquini D. Extraction and characterization of cellulose nanocrystals from agro-industrial residue – Soy hulls. Ind Crops Prod. 2013;42:480-8.
28. Thambiraj S, Shankaran DR. Preparation and physicochemical characterization of cellulose nanocrystals from industrial waste cotton. Appl Surf Sci. 2017;412:405-16.
29. Agarwal J, Mohanty S, Nayak SK. Valorization of pineapple peel waste and sisal fiber: study of cellulose nanocrystals on polypropylene nanocomposites. Applied Polymer Science. 2020;137:1-19.
30. Teodoro KBR, Teixeira EM, Correa AC, Campos A, Marconcini JM, Mattoso LHC. Nanofibras de celulose obtidas a partir de fibras de sisal branqueadas com solução alcalina de peróxido de hidrogênio. In II Jornada cientifica- EMBRAPA; 2010 Set 16-17; São Carlos. Proceedings. São Carlos: Embrapa; 2010. p. 99.
31. Embrapa. Ministério da Agricultura. Pecuária e abastecimento [Internet]. 2022 [cited 2022 June 13]. Available from: https://www.embrapa.br/agencia-de-informacao-tecnologica/cultivos/sisal/pre-producao/socioeconomia/importancia-socioeconomica
32. Mondragon G, SantamariaEchart A, Hormaiztegui MEV, Arbelaiz A, PeñaRodriguez Mucci CV, Corcuera M, et al. Nanocomposites of waterborne polyurethane reinforced with cellulose nanocrystals from sisal fibres. J Polym Environ. 2017;26:1-12.
33. Teodoro KBR, Teixeira EM, Corrêa AC, Campos A, Marconcini JM. Whiskers de fibra de sisal obtidos sob diferentes condições de hidrolise ácida: efeito do tempo e da temperatura de extração. Polímeros. 2011;21:280-5.
34. Abbot S, Holmes N. Nanocoatings: principles and pratice. Pennsylvania: DEStech Publications; 2013
35. Chassaing E, Wiart R. Electrocrystallization mechanism of Zn-Ni alloys in chloride electrolytes. Electrochim Acta. 1992;36:545-53.
36. Franco LA, Sinatora A. 3D surface parameters (ISO 25178-2): Actual meaningof Spk and its relationship to Vmp. Precis Eng. 2015;40:106-11.
37. Ramgir NS, Hwang YK, Mulla IS, Chang JS. Effect of particle size and strain in nanocrystalline SnO2 according to doping concentration of ruthenium. Solid State Sci. 2006;6:359-62.
38. Chopra KL. Thin film phenomena. New York: McGraw-Hill; 1969.
39. Soares ME, Souza CAC, Kuri SE. Corrosion resistance of a Zn-Ni electrodeposited alloy obtained with a controlled electrolyte flow and gelatin additive. Surf Coat Tech. 2006;201(6):2953-9.
40. ASTM: American Society for Testing and Materials. ASTM G31-72: standard practice for laboratory immersion corrosion testing of metals. West Conshohocken: ASTM; 2004.
41. Müller C, Sarret M, Benballa M. ZnNi/SiC composites obtained from an alkaline bath. Surf Coat Tech. 2002;162:49-53.
42. Ghaziof S, Gao W. Zn–Ni–Al2O3 nano-composite coatings prepared by sol-enhanced electroplating. Appl Surf Sci. 2015;351:869-79.
43. Tulio PC, Rodrigues SEB, Carlos IA. The influence of SiC and Al2O3 micrometric particles on the electrodeposition of ZnNi films and the obtainment of ZnNi–SiC and ZnNi–Al2O3 electrocomposite coatings from slightly acidic solutions. Surf Coat Tech. 2007;202:91-9.
44. Karim MRA, Raza SA, Haq EU, Khan KI, Taimoor AA, Khan MI, et al. Electrochemical and thermomechanical behavior of nickel–graphene oxide (2-4L GO) nanocomposite coatings. Appl Phys, A Mater Sci Process. 2021;127(3):1-11.
45. Tsongas K, Tzetzis D, Karantzalis A, Banias G, Exarchos D, Ahmadkhaniha DA, et al. Microstructural, surface topology and nanomechanical characterization of electrodeposited Ni-P/SiC nanocomposite coatings. Appl Sci (Basel). 2019;9:1-16.
46. Zadeh KM, Shakoor RA, Radwan AB. Structural and electrochemical properties of electrodeposited ni–p nanocomposite coatings containing mixed ceramic oxide particles. Int J Electrochem Sci. 2016;11:7020-30.

47. Byk TV, Gaevskaya TV, Tsybulskaya LS. Effect of electrodeposition conditions on the composition, microstructure, and corrosion resistance of Zn–Ni alloy coatings. Surf Coat Tech. 2008;202:5817-23.
48. Anwar S, Khan F, Zhang Y. Corrosion behaviour of Zn-Ni alloy and Zn-Ni-nano-TiO2 composite coatings electrodeposited from ammonium citrate baths. Process Saf Environ Prot. 2020;141:366-79.
49. Sudhakar R, Venkatesh VT. Electrodeposition of Zn–Ni multiwalled carbon nanotube nanocomposites and their properties. Ind Eng Chem Res. 2013;52:6422-9.
50. Hammami O, Dhouibi L, Berçot P, Rezrazi EM, Triki E. Study of Zn-Ni alloy coatings modified by nano-SiO2 particles incorporation. Int J Corros. 2012;2012:301392.
51. Kumar CMP, Lakshmikanthan A, Chandrashekarappa MPG, Pimenov DY, Giasin K. Electrodeposition based preparation of Zn–Ni Alloy and Zn–Ni–WC nano-composite coatings for corrosion-resistant applications. Coatings. 2021;11:1-17.
52. Low CTJ, Wills RGA, Walsh FC. Electrodeposition of composite coatings containing nanoparticles in a metal deposit. Surf Coat Tech. 2006;201:371-83.
53. Alipour K, Nasirpouri F. Smart anti-corrosion self-healing zinc metal-based molybdate functionalized-mesoporous-silica (MCM-41) nanocomposite coatings. RSC Advances. 2017;7:51879-87.
54. Daneshvar-Fatah F, Nasirpouri F. A study on electrodeposition of Ni-noncovalnetly treated carbon nanotubes nanocomposite coatings with desirable mechanical and anti-corrosion properties. Surf Coat Tech. 2014;248:63-73.
55. Xing S, Wang L, Jiang C, Liu H, Zhu W, Ji V. Influence of Y2O3 nanoparticles on microstructures and properties of electrodeposited Ni–W–Y2O3 nanocrystalline coatings. Vacum. 2020;181:1-10.
56. Montero-Ocampo C, Veleva L. Effect of cold reduction on corrosion of carbon steel in aerated 3% sodium chloride. Corros. 2002;58:601-7.
57. Doolabi MS, Sadrnezhaad SK, Doolabi DS, Asadirad M. Influence of pulse parameters on electrocodeposition of Cr–Al2O3 nanocomposite coatings from trivalent chromium bath. Int Heat Treat Surf Eng. 2012;6:178-84.
58. Vaezi MR, Sadrnezhaad SK, Nikzad L. Electrodeposition of Ni–SiC nano-composite coatings and evaluation of wear and corrosion resistance and electroplating characteristics. Colloids Surf A Physicochem Eng Asp. 2008;315:176-82.
59. Sajjadnejad M, Setoudeh N, Mozafari A, Isazadeh A, Omidvar H. Alkaline electrodeposition of Ni–ZnO nanocomposite coatings: effects of pulse electroplating parameters. Trans Indian Inst Met. 2017;70:1533-41.
60. Feng Z, Li Q, Zhang J, Yang P, An M. Studies on the enhanced properties of nanocrystalline Zn-Ni coatings from a new alkaline bath due to the additives. RSC Advances. 2015;5(72):58199-210.
61. Vlasa A, Varvara S, Pop A, Bulea C, Muresan LM. Electrodeposited Zn–TiO2 nanocomposite coatings and their corrosion. J Appl Electrochem. 2010;40:1519-27.
62. Zhang XG. Corrosion and electrochemistry of zinc. Boston: Springer; 1996. Corrosion potential and corrosion current; p. 125-156.
63. Close D, Stein N, Allain N, Tidu A, Drynski E, Merklein M, et al. Electrodeposition, microstructural characterization and anticorrosive properties of Zn-Mn alloy coatings from acidic chloride electrolyte containing 4-hydroxybenzaldehyde and ammonium thiocyanate. Surf Coat Tech. 2016;298:73-82.
64. Hashimoto S, Abe M. The characterization of eletrodeposited Zn-SiO and composites before and afer corrosion test. Corros Sci. 1994;36:2125.
65. Mouanga M, Puiggali M, Devos O. EIS and LEIS investigation of aging low carbon steel with Zn–Ni coating. Electrochim Acta. 2013;106:82-90.
66. Chen C, Qiu S, Cui M, Qin S, Yan G, Zhao H, et al. A Achieving high performance corrosion and wear resistant epoxy coatings via incorporation of noncovalent functionalized graphene. Carbon. 2017;114:356-66.
67. Gu C, Lian J, He J, Jiang Z, Jiang Q. High corrosion-resistance nanocrystalline Ni coating on AZ91D magnesium alloy. Surf Coat Tech. 2006;200:5413-8.
68. Azar MMK, Gugtapeh HS, Rezaei M. Evaluation of corrosion protection performance of electroplated zinc and zinc-graphene oxide nanocomposite coatings in air saturated 3.5 wt. % NaCl solution. Colloids Surf A Physicochem Eng Asp. 2020;601:12501.
69. Li S, Song G, Zhang Y, Fu Q, Pan C. Graphene reinforced Zn–Ni Alloy composite coating on iron substrate by pulsed-reverse electrodeposition and its high corrosion resistance. ACS Omega. 2021;21:13728-41.
70. Alipour K, Nasirpouri F. Effect of morphology and surface modification of silica nanoparticles on the electrodeposition and corrosion behavior of zinc-based nanocomposite coatings. J Electrochem Soc. 2019;166:1-9.
71. Zheng H, An M, Lu J. Corrosion behavior of Zn-Ni-Al2O3 composite coating. Rare Met. 2006;25:174-8.
72. Zadeh KM, Shakoor RA, Radwan AB. Structural and electrochemical properties of electrodeposited Ni–P nanocomposite coatings containing mixed ceramic oxide particles. Int J Electrochem Sci. 2016;11:7020-30.
73. Zheng H, An M. Electrodeposition of Zn–Ni–Al2O3 nanocomposite coatings under ultrasound conditions. J Alloys Compd. 2008;459:548-52.
74. Praveen BM, Venkatesha TV. Electrodeposition and corrosion resistance properties of Zn-Ni/TiO2 Nano composite coatings. Int J Electrochem. 2011;261:407.
75. Ghorbani M, Saleh F, Razavizadeh O. Enhanced hardness and corrosion resistance of Zn/SiO2 films by electrodeposition. J Electrochem Soc. 2015;162:D-480-D485.
76. Mokabber T, Rastegari S, Razavizadeh H. Effect of electroplating parameters on properties of Zn–nano-TiO_2 composite coatings. Surf Eng. 2013;29:41-5.
77. Klekotka M, Zielinska K, Stankiewicz A, Kuciej M. Tribological and anticorrosion performance of electroplated zinc based nanocomposite coatings. Coatings. 2020;10:594.
78. Praveen BM, Venkatesha TV. Electrodeposition and properties of Zn-nanosized TiO2 composite coatings. Appl Surf Sci. 2008;254:2418-24.